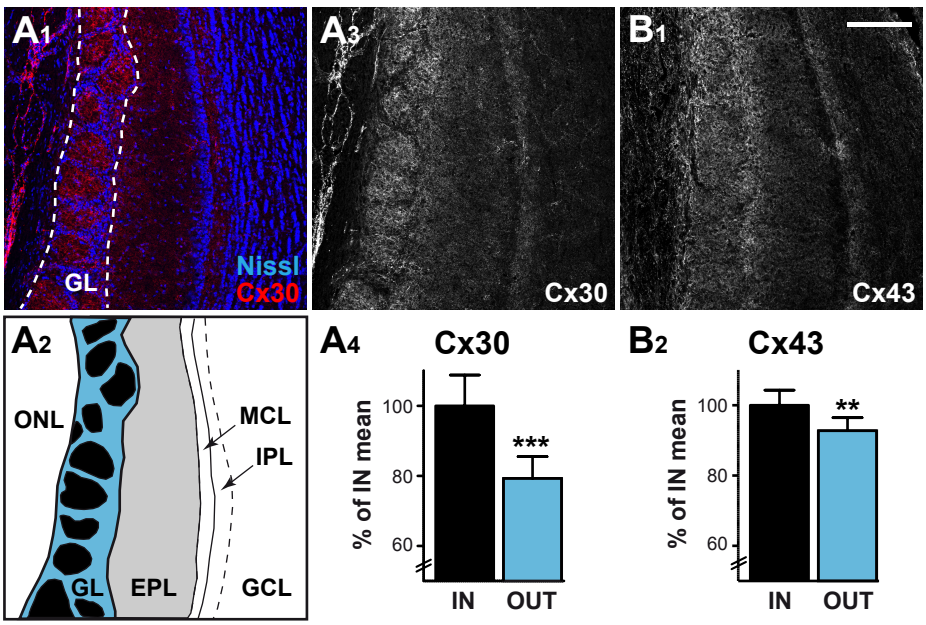

Fig. S1. Expression of the two astroglial connexins in the glomerular layer at P20. **A1,A3:** Low magnification images of Cx30 immunostaining (red in A1) in the olfactory bulb indicate an enriched expression of this Cx in the glomerular layer (GL, delimited by dotted lines in A1) compared to the surrounding layers identified by a Nissl counterstaining (blue in A1). **A2:** Scheme representing the different regions of the olfactory bulb corresponding to the image presented in A1. ONL, Olfactory Nerve Layer; EPL, External Plexiform Layer; MCL, Mitral Cell Layer; IPL, Internal Plexiform Layer; GCL, Granule Cell Layer. **A4:** Within the glomerular layer, quantification of the mean immunofluorescence intensity indicates that Cx30 expression is significantly higher ($P<0.0001$, $n=10$) within the glomeruli (IN, black in A2) compared to the extraglomerular area (OUT, blue in A2). Results are expressed in function of the mean fluorescence measured in the glomerular area. **B1-B2:** Low magnification images of Cx43 immunostaining show an enriched expression at the limit between the GL and the EPL. **B2:** Within the glomerular layer, quantification of the mean immunofluorescence intensity indicates that Cx43 expression is significantly higher ($P<0.001$, $n=10$) within the glomeruli compared to the extraglomerular area. Scale bar: 100 µm.

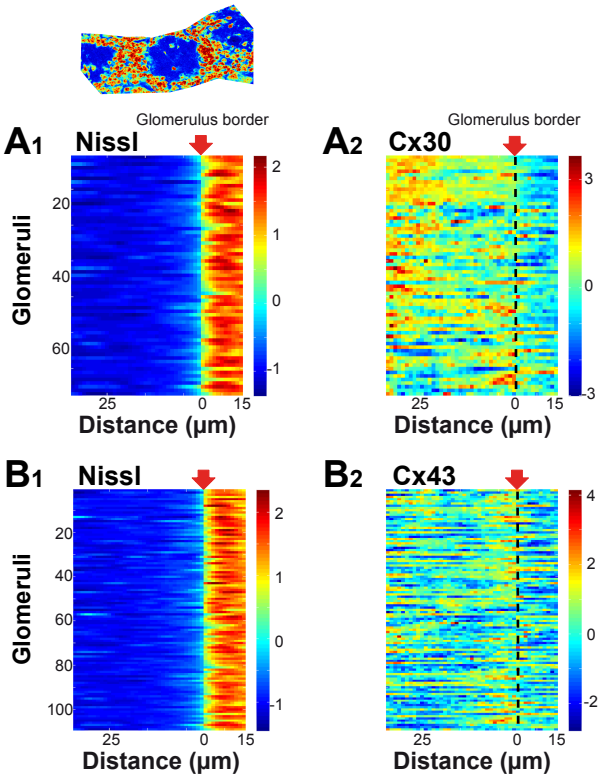

Fig. S2. Differential expression of the two astroglial connexins at glomerular border at P20. Analysis of Cx expression at the border of a glomerulus: the mean fluorescence intensity of the different stainings was measured in each 1µm-large concentric rings designed from the glomerulus border (determined with the Nissl staining, example on top left), within and outside the glomeruli. Each line represents results obtained for one glomerulus, each column corresponds to one ring (see SI Methods). Results are expressed in Zscores in order to pool the data obtained from different immunostainings. **A1, B1:** Results obtained for the Nissl counterstaining are shown as control: using this representation the olfactory glomeruli borders (red arrows, dotted line in A2 and B2) are clearly visible. **A2, B2:** Data, obtained from 67 glomeruli and 109 glomeruli for the Cx30 (A2) and the Cx43 (B2), respectively, indicates that both Cxs are less expressed outside glomeruli. Interestingly, Cx30 and Cx43 show different patterns of expression within the glomeruli. Averaged results and statistics are shown in Figure 1 D. Similar results were obtained in adult tissues.

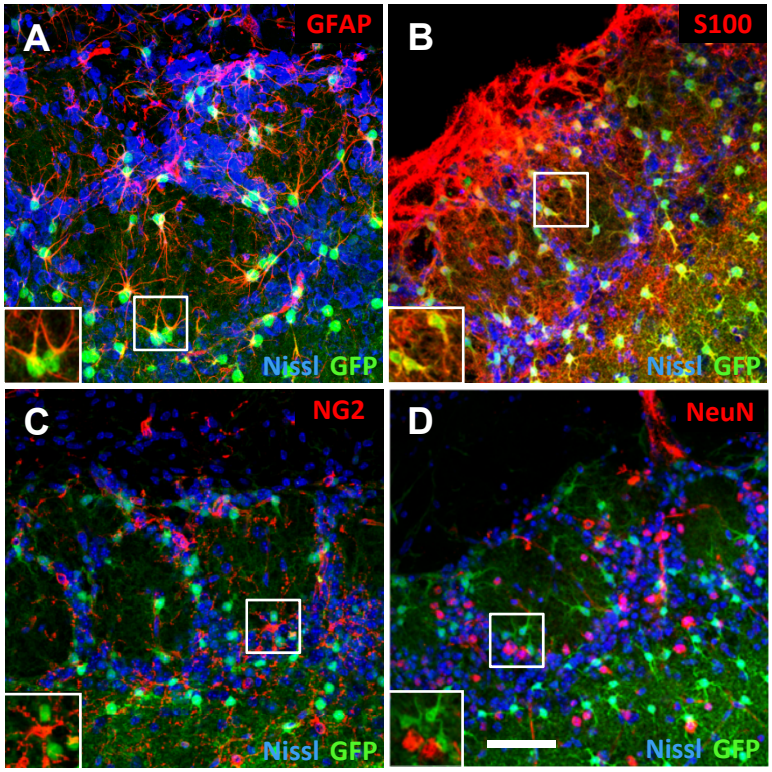

Marker	% of colocalization with GFP
GFAP	96% (n=421 cells)
S100	99% (n=271 cells)
NG2	0,4% (n=375 cells)
NeuN	0% (n=246 cells)

Fig. S3. GLT1-eGFP BAC reporter mice as a tool to study gap junctional communication in the glomerular layer. Immunostainings with different brain cell type markers were performed on GLT1-eGFP BAC reporter mice tissues: GFAP (A) and S100 (B) for astrocytes, NG2 (C) for oligodendrocytes precursors, and NeuN (D) for neurons. Nissl staining was used for counterstaining all cells to identify the location of olfactory glomeruli. Squares indicate the zones for which a high magnification is shown in inset. Scale bar: 50µm. The percentages of colocalization of the different markers with the GFP+ cells are summarized in the Table and indicate that GLT1-eGFP positive cells mostly correspond to astrocytes.

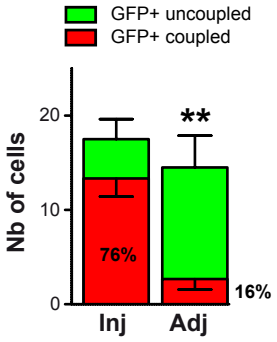

Fig. S4. Orientation of dye coupling in the GLT1-eGFP BAC reporter mice. For each injection of glomerular astrocyte, the number of GFP+ astrocytes located within the injected glomerulus (Inj) or in adjacent glomeruli (Adj) was determined within a fixed volume around the injected cell (SI Methods). They constitute a pool of potential "receiver" cells for the dye. This analysis shows that 76±6% of these astrocytes located in the same glomerulus than the injected cell are coupled to this latter whereas only 16±5% of the astrocytes from adjacent glomeruli receive the dye (A) (n=6 injections, **P<0.01, chi-square test). The pools of candidates are similar for the two locations considered (Inj or Adj) (P=0.47, n=6). Within these pools, the number of GFP+ cells that effectively received the dye is represented in red while the uncoupled GFP+ cells left are represented in green.

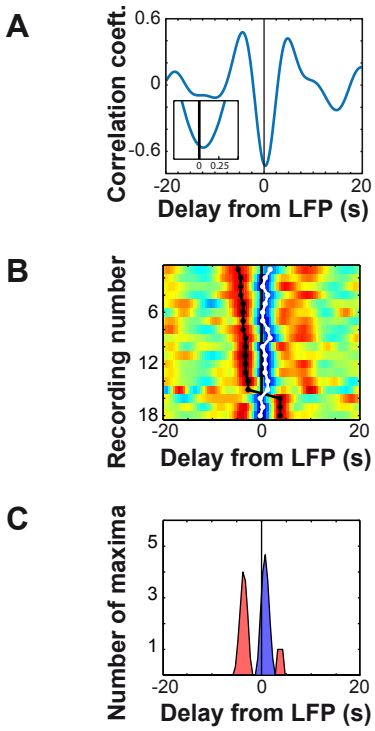

Fig. S5. Membrane potential fluctuations in astrocytes and local field potentials recorded from the same olfactory glomerulus are correlated. **A:** Membrane potential monitored by whole-cell recording of a glomerular astrocyte and local field potential (LFP) measured in the same glomerulus exhibited correlated fluctuations in the range of 0.05-0.2Hz. Cross-correlogram analysis applied to the two signals shown in the example of Fig. 3C, filtered in the 0.05-0.2Hz frequency band, indicates a zero-lag correlation coefficient of -0.7 ($P<0.01$) (LFP being used as reference). Insert: high magnification of the curve around zero lag highlights that astrocyte signal is delayed by 300ms compared to the LFP (lag corresponding to the maximal negative value of the correlation coefficient). Averaged cross-correlogram curve obtained for 18 similar recordings is presented in Figure 3D. **B:** Results of this cross-correlogram analysis performed on 18 recordings sessions are presented in Z-scores (each line for one recording). Colors ranging from red to blue correspond to strong positive or negative correlation, respectively. This analysis reveals all the analyzed astrocytes were negatively correlated with the LFP (blue color at zero lag). Joined dots indicate maximal positive (black) or negative (white) values of the correlation coefficient close to zero lag. **C:** Distribution of the maxima obtained for positive (red) and negative (blue) correlation close to zero lag.

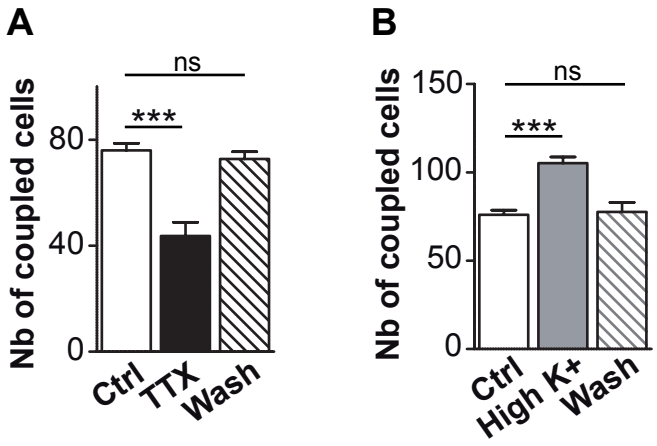

Fig. S6. Reversibility of TTX and high potassium treatments on glomerular network communication. **A:** The 43% inhibition of the dye coupling induced by at least 1h of TTX treatment (n=12) was totally reversed by washing the slice for at least 2h in normal ACSF (n=4). This effect was associated with the recovery of neuronal spiking recorded in mitral cells (n=3). **B:** The 39% increase in dye coupling induced by few minutes of high K+ treatment (n=4) was totally reversed by washing the slice for at least 1h (n=7).

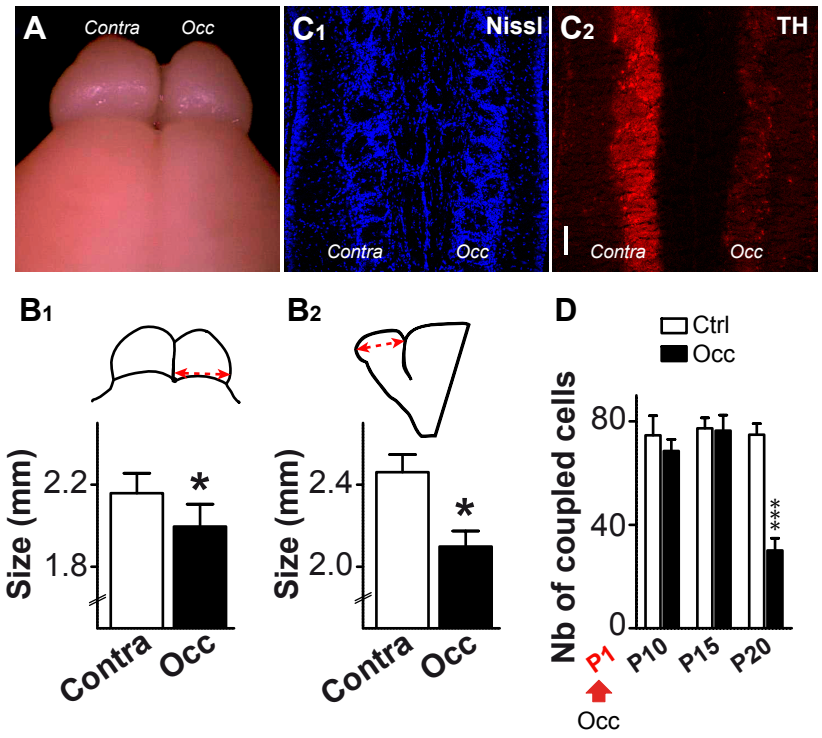

Fig. S7. Effect of early olfactory deprivation. **A:** Unilateral naris occlusion performed at P1 resulted in a decrease in size of the ispsilateral olfactory bulb at P20. **B1-B2:** Quantification of the size reduction measured in the horizontal and sagittal directions (red arrows) of the olfactory bulb (in B1: n=5, $P<0.05$; in B2: n=3, $P<0.05$, Wilcoxon signed rank test). **C1-C2:** Early olfactory deprivation resulted in a strong decrease in tyrosine hydroxylase (TH) immunoreactivity in the glomerular layer of the deprived bulb (C2; occ), delimited by Nissl staining (C1). Scale bar: 100µm. **D:** Olfactory deprivation performed at P1 resulted in a significant reduction of dye coupling at P20 (n=10 and 9 at P20 for control and occluded conditions, respectively, $P<0.001$) but not before (n=7 and 4 at P10; n=14 and 7 at P15; for control and occluded conditions, respectively, $P>0.5$). This time schedule corresponds to the appearance of the Cx30 in the brain.

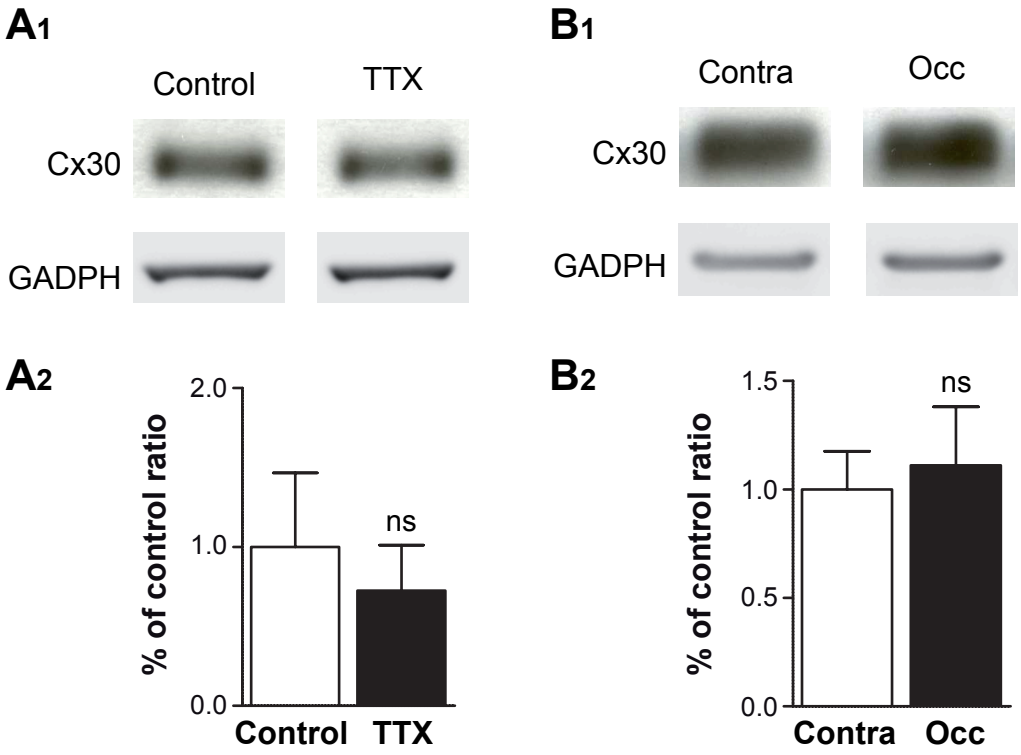

Fig. S8. The expression of Cx30 in the olfactory bulb is not affected by TTX pharmacological treatment or early olfactory deprivation. **A1-B1:** Examples of immunoblots for Cx30 after TTX treatment (0.5 µM, 1h minimum) (A) and naris occlusion (Occ, B) with their internal controls (control without TTX, and contra, contralateral unoccluded bulb). **A2-B2:** Results, expressed as the percentage of control ratio obtained with GADPH, show no significant effect induced by the two different protocols (P=0.37,n=4; P=0.62, n=6; for TTX treatment and sensory deprivation, respectively, Wilcoxon signed rank test).

SI Methods

All animal protocols were approved by the European Community Council Directives of November 24th, 1986 (86/609/EEC) and followed INSERM guidelines for the ethical treatment of animals.

Animals

C57BL/6 mice (Charles River Laboratories) were used as wild-type mice. Transgenic mice expressing eGFP in astrocytes were also used: [human glial fibrillary acidic protein (hGFAP)]-eGFP mice (1) and the [glutamate transporter-1 (GLT-1)]-eGFP BAC reporter mice (2). Knockout mice, including $Cx30^{-/-}$ (KOCx30) (3), $Cx43^{fl/fl}$:GFAP-cre (KOCx43), a conditional knockout of Cx43 in astrocytes (4) and the double knockout $Cx30^{-/-}$ $Cx43^{fl/fl}$:GFAP-cre (5) were used.

Analysis of astrocyte morphologies

Vectorial analysis of astrocyte morphologies

In hGFAP-eGFP mice, a vector with a fixed norm was attributed to each of the primary processes of the considered astrocyte (see schemes below).

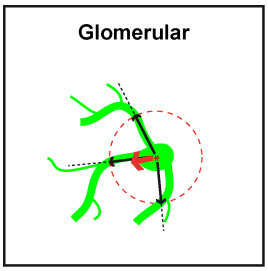

The average vector corresponding to the so-obtained vectors (red) was then calculated and the scalar product between this averaged vector and the vector drawn from the astrocyte soma to the glomerulus center was calculated.

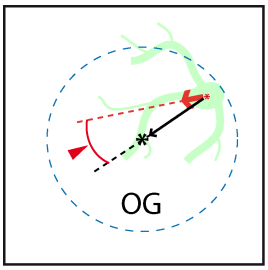

The so-calculated angle gives the global direction of the processes with regard to the glomerulus center. Statistical significance was assessed by comparing the angle distribution obtained for several OG astrocytes to a Gaussian distribution with an identical standard deviation aligned on a zero angle.

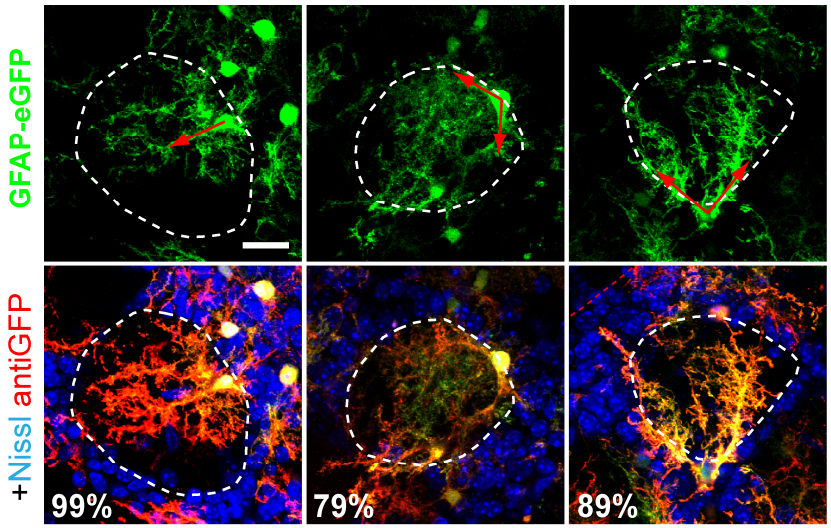

Examples of hGFAP-eGFP+ glomerular astrocytes (*top*, green) with amplification provided by anti-GFP antibodies (*bottom*, red). Nissl staining is used to define glomerular boundaries (bottom, blue). Scale bar: 20µm. Red arrows indicate the directions of the primary processes used to calculate the averaged vector.

Analysis of OG astrocyte process distribution

Immunohistochemistry using anti-GFP antibodies on tissues from hGFAP-eGFP mice was performed in association with a Nissl staining to delimit glomerular boundaries. This allowed determining the percentage of anti-GFP immunofluorescence measured on astroglial processes located within OG. Results obtained for the anti-GFP immunofluorescence (85±6%, n=4) and for the GFP (89±4%, n=4) were similar (P=0.12, Wilcoxon matched pairs test) and both indicate that most of OG astrocyte processes are intraglomerular. Alternatively, the percentage of the total number of primary processes was measured for each glomerular astrocyte.

Immunohistochemistry

Antibodies

The following primary antibodies were used: polyclonal rabbit antibodies anti-Cx30, anti-Cx43 (1:500; Zymed for both), anti-S100 (1:4000; BD Biosciences), anti-NG2 (1:400; Millipore Bioscience Research Reagent), anti-TH (1:500 Chemicon), anti-GFP (1:500; Invitrogen); monoclonal mouse antibodies anti-NeuN (1:500; Millipore Bioscience Research Reagent) and anti-GFAP (1:500; Inc. Biomedicals, clone GA-5). Goat anti-rabbit or mouse Igs conjugated to Alexa fluor dyes (1:4000; Molecular Probes) were used in appropriate combinations as secondary antibodies.

Protocols
Cxs-stainings:
P20 mice were anesthetized with pentobarbital injection, perfused with PBS and their brains were rapidly removed and frozen in isopentane cooled at -30°C. Coronal sections (20 µm) were cut with a cryostat, collected on slides and fixed with 2% paraformaldehyde in PBS for 10 minutes at 4°C. Sections were permeabilized in PBS containing 0.2 % gelatin and 0.2% Triton-X100 (PBS*) for 1 hour and processed for simple or double immunostaining by overnight incubation at 4°C with rabbit anti-Cx antibodies and/or mouse anti-GFAP antibodies diluted in PBS*. After 2 washes (30 minutes each), sections were incubated for 2 hours at room temperature with appropriate secondary antibodies. After 2 washes (20 minutes each), Nissl counterstaining was performed by incubating the sections during 20 minutes in Neurotrace reagent (1:100 Invitrogen) diluted in PBS. Sections were mounted in Fluoromount and imaged with a confocal laser-scanning microscope, equipped with a 63x or a 40x objective and three lasers (argon 488 nm, helium/neon 543 nm, helium/neon 633 nm).

Post-recording TH stainings, GFP signal amplification in hGFAP-eGFP mice, GLT1-eGFP BAC reporter mice characterization:
After after slicing or whole-cell recording, 300µm thick slices were fixed overnight in 4% paraformaldehyde in PBS at 4 °C. Then after 2 PBS washes (20 minutes each), slices were permeabilized with PBS* for 1 hour at room temperature followed by overnight incubation at 4 °C with rabbit anti-TH, anti-GFP, anti-GFAP, anti-S100, anti-NeuN or anti-NG2, diluted in PBS*. Slices were then processed like previously described for Cx-stainings.

Analysis of Cx immunostainings

Low magnification analysis on the glomerular layer
Nissl staining was used to delimit the glomerular layer and the glomerular boundaries on confocal images acquires with a 20x objective (see Fig. S1). In a number of frames corresponding to single confocal sections (12 for Cx43 and 11 for Cx30), the mean intensity of Cx immunofluorescence was measured in the glomerular and the extraglomerular areas (see Fig. S1 A2). However, this method could possibly be biased by the fact that extraglomerular locations may belong to the edge of a glomerulus located above or below the confocal plan in 3D. Moreover, the limit between the GL and the EPL was not always clearly visible and the considered extraglomerular area may contain portion of the EPL. To avoid these biases, we completed our study by the following analysis.

High magnification analysis at the glomerulus border
Cx immunoreactivity was measured in 1µm-large concentric rings defined from the glomerulus border (see scheme below), delimited by a Nissl counterstaining as before. 10µm outside and 30µm inside the glomerulus were considered for the analysis.

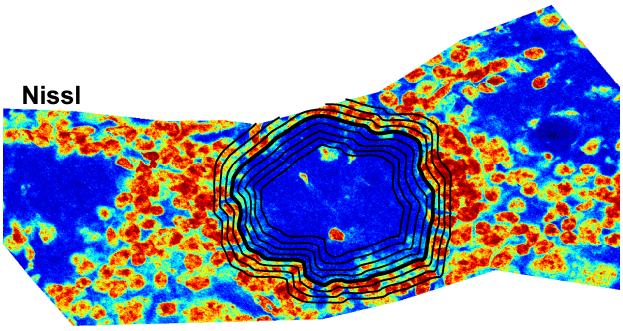

Note that for clarity only few rings were represented in this picture.

The results were expressed in Z-scores (variations from the mean value of the entire frame) in order to pool the data obtained for numerous glomeruli obtained from different immunostainings. The results obtained for 109 glomeruli are individually represented in Figure S2. The data obtained for the Nissl staining allowed us to control that the glomerular boundaries were correctly delimited as a clear drop in the values was obtained at the transition between the glomerular and the extraglomerular areas (Fig. S2 A1 and B1). Averaged results calculated for Cx immunostainings are illustrated in Figure 1 D.

Tissue preparation for electrophysiology

Mice [postnatal day (P)]1 to 23 were killed by decapitation, and the bulbs were rapidly dissected in ice-cold oxygenated (95% O2–5% CO2) solution containing (in mM): 83 NaCl, 26.2 NaHCO3, 1 NaH2PO4, 2.5 KCl, 3.3 MgSO4, 0.5 CaCl2, 70 sucrose, and 22 D-glucose, pH 7.3 (osmolarity 315mOsm). Horizontal slices (250-350µm) were cut using a Microm HM 650 V vibratome in the same solution, incubated for 30-40 min at 34°C in the standard extracellular solution (see below) in which 10mM of pyruvate was added, and stored at room temperature until use (up to 5 hours after decapitation).

Electrophysiology and dye coupling experiments

For dye coupling experiments, slices were placed in a submerged recording chamber mounted on a microscope (Zeiss Axioskop FS) equipped for infrared-differential interference (IR-DIC) microscopy. They were perfused continuously with oxygenated extracellular solution containing (in mM): 124 NaCl, 26 NaHCO3, 3 KCl, 1.25 NaH2PO4, 1.3 MgCl2, 2 CaCl2, and 20 D-glucose (pH 7.4, room temperature), perfused at a rate of 2 ml/min. Cells in the glomerular layer were identified as astrocytes based first on their morphology and second on their electrophysiological properties. Patch-clamp recordings were performed with 3-7 MΩ glass electrodes filled with (in mM): 105 K-gluconate, 30 KCl, 10 HEPES, 10 phospho-creatine, 4 ATP-Mg, 0.3 GTPTris, 0.3 EGTA (pH 7.4, 290 mOsm). Whole-cell membrane voltages and currents were amplified by a MultiClamp 700B amplifier, sampled by a Digidata 1322A Interface, and recordings (10 kHz sampling, 2kHz filtering) were performed with Pclamp9 software (Molecular Devices). Series resistances were compensated at 80%. Input resistance was measured in

voltage-clamp mode by applying hyperpolarizing voltage pulses (10 mV, 150 ms) from a holding potential of -80 mV.

To evaluate the level of coupling, sulforhodamine B (SrB) (1 mg/ml; Invitrogen) and dextran tetramethylrhodamine (1 mg/ml; Invitrogen) were added to the internal solution. Recorded cells were loaded with these molecules during 20 minutes in current-clamp mode and only cells recorded with an input resistance under 50MΩ were considered for analysis. Intercellular diffusion of fluorescent molecules was captured online at different focal plans with a digital camera (PixelFly) at the end of astrocyte dialysis and the number of coupled cells was analyzed off-line with Image J software. For some experiments, slices underwent pretreatments that were maintained during recordings: 0.5µM TTX or 200µM barium were applied for 1 to 3 hours, 6mM $[K^+]_e$ ACSF for at least 10 minutes before recording. Recoveries experiments were performed after at least one hour of washout in normal ACSF for 6mM $[K^+]_e$. After TTX treatment, at least two hours of washout were required to observe a recovery of spiking activity in MCs.

Coupling distribution analysis

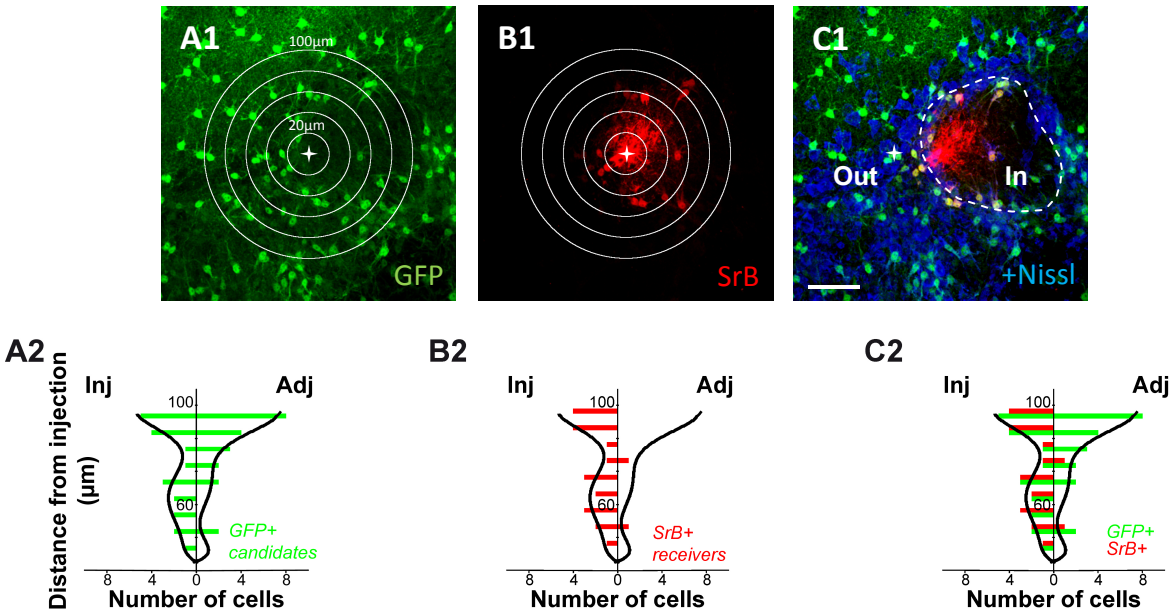

Dye coupling experiments were performed as described above, in GLT-1-eGFP mice BAC reporter mice (2). After SrB dialysis (B_1, red), slices were fixed in 4% paraformaldehyde in PBS overnight at 4 °C. After 2 PBS washes, permeabilization and Nissl staining (C_1, blue), images were acquired with a confocal microscope (Leica TCS SP5). *Scale bar: 50µm*. Following this procedure, the number of detectable coupled cells was reduced by ~60% compared to the coupling observed on line ($P<0.001$). In the GLT-1-eGFP mice BAC reporter mice model, most of astrocytes were GFP^+ (see Fig. S3). Around the injected cell, it was then possible to visualize astrocytes that could potentially receive the dye. The number of GFP^+ candidates was calculated in 3D for a

range of distances within the injected glomerulus (Inj) or in adjacent glomeruli (Adj) (Fig. A_{1-2}). To do so, the distance from the injection site was measured and the location (Inj or Adj) was determined for each of them. The same analysis was performed for SrB^+ coupled cells (Fig. B_{1-2}). Data were pooled for 6 glomerular injections to have a global insight on the spatial organization of the coupling (Fig. 2 A_2,B_2). The comparison between the distributions obtained for GFP^+ 'candidates' and SrB^+ 'receivers' allowed to determine the likelihood of an astrocyte to be coupled, with respect to its location. For example, nearly all glomerular GFP^+ candidates were coupled while many candidates located in adjacent glomeruli were not loaded, even though they were located as far as the coupled glomerular astrocytes from the injection (Fig. C_{1-2}). This indicates that the probability for a glomerular astrocyte to be coupled to an astrocyte from the same glomerulus is higher than to an astrocyte located in adjacent glomeruli at the same distance from the injection. In other words it is not primarily the distance of a recipient cell that determines whether it is coupled or not, but rather its location within the injected glomerular or other glomeruli.
Complementarily, the number of GFP^+ astrocytes located within the injected glomerulus or in adjacent glomeruli was determined within a fixed volume around the injected cell, without considering the distance from the injection site (Fig. 2 C, Fig. S4). The percentage of these GFP^+ candidates that were effectively coupled (SrB^+) was then determined in each locations (Inj or Adj). A chi-square test was used to compare the percentages of coupled GFP^+ cells in these two locations. Notably, the denominators (total number of GFP^+ candidates) were similar in these two areas (Fig. S4; P=0.47, n=6).

Analysis of electrophysiological recordings

Astrocyte membrane potential analysis

Whole-cell astrocyte recordings were performed at the same time as dye coupling experiments. Analysis was performed using Matlab software. Recordings were acquired at 10kHz, then re-sampled and the baseline was adjusted with a method that exploits the crossover of moving averages (6). As described by (7), the standard deviation of the membrane potential (Vm) distribution was used as an indicator of fluctuations amplitude.

Cross-correlogram

The temporal relationship between astroglial Vm fluctuations and LFP signals recorded in the same glomerulus (less than 40µm from astrocyte cell body) were investigated by cross-correlogram with custom-written, MATLAB-based programs (MathWorks, Natick, MA, USA). A significant value for the correlation coefficient (r) at the lag zero indicates that the two signals do not evolve independently. We defined the delay between the 2 signals as the lag corresponding to the time delay that optimizes the correlation between them. We performed cross-correlogram analysis on 18 recordings filtered in the 0.05-0.2 Hz frequency band. Results are consistent with those reported previously in the cortex (7).

Naris occlusions

As already described (8), mice at the age of P1 were deeply anesthetized by hypothermia and their right external naris was briefly cauterized. The scar was disinfected locally to avoid post procedural infection and a Lidocaine gel was applied to reduce pain. The pup was then kept warm for 1 hour and returned to its cage. The efficacy of the occlusion formed by the scar tissue was examined every two days, by verifying the absence of bubble when a drop of water was applied on the closed naris. This protocol results in blocking airflow over the ipsilateral mucosa without directly damaging the olfactory receptors that reside in the posterior portion of the nasal cavity. After dye coupling experiments, a tyrosine hydroxylase (TH) immunohistochemistry was performed on the fixed slices to validate occlusion success (Fig.S4 A) (9).

Immunoblottings

Frozen brain hemispheres samples were pulverized using a mortar and pestle on dry ice, resuspended in boiling 2% SDS containing a cocktail of protease inhibitors (Boehringer), ß-glycerophosphate (10 mM) and orthovanadate (1 mM), and sonicated on ice. Brain extracts were centrifuged 20 minutes at 13 000 rpm at 4°C and supernatants were collected to which 5x Laemmli buffer was added and boiled 5 minutes. Proteins were quantified using the BCA protein assay kit (Pierce). Protein samples (20 µg/lane) were separated by electrophoresis on 10% polyacrylamide gels and transferred onto nitrocellulose membranes. Membranes were saturated with 5% fat-free dried milk in triphosphate buffer solution supplemented with tween 0,1% and incubated overnight at 4°C with primary antibodies : anti- Cx30 (mouse monoclonal Lifespan Biosciences; 1/500), diluted in the same buffer. They were then washed and exposed to peroxidase-conjugated goat anti-mouse IgG (1/2500, Santa Cruz Biotech). Specific signals were revealed with the chemiluminescence detection kit (ECL, GE Healthcare). Blots were reprobed with mouse monoclonal anti-GAPDH-peroxidase (Sigma, 1/10000) to check for protein load. Semiquantitative densitometric analysis was performed with imageJ software after scanning the bands.

Statistics

For each data group, results are expressed as mean ± SEM and n refers to the number of independent experiments. Unless mentioned, unpaired two-tailed student test was used. Differences are considered significant at *P<0.05, **P<0.01 and ***P<0.001. GraphPad Prism 5 or Matlab software (MathWorks, Natick, MA, USA) were used for calculations.

References

1. Nolte C*, et al.* (2001) GFAP promoter-controlled EGFP-expressing transgenic mice: a tool to visualize astrocytes and astrogliosis in living brain tissue *Glia* **33,** 72-86.
2. Regan MR*, et al.* (2007) Variations in promoter activity reveal a differential expression and physiology of glutamate transporters by glia in the developing and mature CNS *J Neurosci* **27,** 6607-6619.
3. Teubner B*, et al.* (2003) Connexin30 (Gjb6)-deficiency causes severe hearing impairment and lack of endocochlear potential *Hum Mol Genet* **12,** 13-21.
4. Theis M*, et al.* (2003) Accelerated hippocampal spreading depression and enhanced locomotory activity in mice with astrocyte-directed inactivation of connexin43 *J Neurosci* **23,** 766-776.
5. Wallraff A*, et al.* (2006) The impact of astrocytic gap junctional coupling on potassium buffering in the hippocampus *J Neurosci* **26,** 5438-5447.
6. Seamari Y, Narvaez JA, Vico FJ, Lobo D, & Sanchez-Vives MV (2007) Robust off- and online separation of intracellularly recorded up and down cortical states *PLoS One* **2,** e888.
7. Mishima T & Hirase H (2010) In vivo intracellular recording suggests that gray matter astrocytes in mature cerebral cortex and hippocampus are electrophysiologically homogeneous *J Neurosci* **30,** 3093-3100.
8. Meisami E (1976) Effects of olfactory deprivation on postnatal growth of the rat olfactory bulb utilizing a new method for production of neonatal unilateral anosmia *Brain Res* **107,** 437-444.
9. Baker H (1990) Unilateral, neonatal olfactory deprivation alters tyrosine hydroxylase expression but not aromatic amino acid decarboxylase or GABA immunoreactivity *Neuroscience* **36,** 761-771.